ECOLE POLYTECHNIQUE
DEPARTMENT OF MECHANICS
Master 2 of Solid Mechanics (4MS)
Multiscales and Multiphysics Modeling of Materials and Structures

Modeling and numerical simulation of the path of a single crack in an elastic material submitted to a stress gradient

Huang Yunfei

Thesis

Master Solid Mechanics-Multiscales and Multiphysics Modeling of Materials and Structures

Ecole polytechnique

Project Advisor:

- Dr. Herve Henry, Laboratory PMC

LABORATOIRE PMC

LMS

Abstract

This work starts the phase field modeling that is a linearized elastodynamics model coupling the phase theory, the material is intact by $\phi = 1$ and crack by $\phi = 0$. This problem is solved by the numerical methods and FORTRAN program.

Firstly we simulate a simple case only the displacement loading and the results are straight crack and symmetric branched crack under the different amplitude of displacement.

Then, the main works are simulations of quasistatic under the thermal loading. There are straight propagation and oscillating propagation with different amplitude of the temperature. Those results fit other experimental and numerical research. The wavelength of oscillating is about 60 and amplitude of oscillating is 25. When the g = 545, the oscillating crack would propagate a little back and it is going on oscillating propagation.

Acknowledgements

First of all, I would like to express my gratitude to my supervisor, Dr. Herve Henry, whose expertise, understanding, and patience, added considerably to my graduated experience. I appreciate his vast knowledge and skills in mathematics, physics and programming. I get lot of knowledge of the phase modeling in this internship, especially, the skill of coding. And he is a kind person that he helps to write some recommendations to help to find the PhD position. Thanks too much for his help.

Besides my advisor, special thanks go out to Professor Marigo Jean-Jacques for his potent recommendation to help to find the PhD position. He has had patient to help me from my master application to my final presentation of the master. And I also have learnt what a good leader is.

I would like to thank all courses of Professors that Mathis Plapp, Yongjun He, Michel Jabbour, Andrei Constantinescu, Patrick Le Tallec, Olivier Pantz, François Alouges, Michel Bornert and Lev Truskinovsky. They are really good in the mechanics and I am improved too much in this year.

I also would like to thank my classmates and good friends, Liu Shu, Sivaprasath Manivannan, Laurent Guin and Saurav Aryan, who helped me so much in learning and living in Ecole P olytechnique. I sincerely wish a good future for all of them.

I would also like to thank my family for the support they provided me through my entire life and in particular.

Contents

1 Introduction **2**

2 Phase-field model and numerical method **5**

2.1 The phase field modeling 5

2.2 Numerical analysis of the evolution problem 7

2.2.1 Initial all fields 8

2.2.2 Current all fields 13

3 The simple case of crack propagation under displacement loading **15**

3.1 Introduction of simulation 15

3.2 The results of simulation 16

4 The dynamics of quasistatic of crack propagation **20**

4.1 Introduction of simulation 20

4.2 Straight crack propagation 22

4.3 Oscillating crack propagation 24

5 Conclusions **29**

Bibliography **30**

Chapter 1
Introduction

The study of fracture is an old topic and the crack formation, propagation, morphology and the path prediction are hot research fields. Especially, the brittle material such as the glass is broken under the thermal loading. This problem would be studied by experimental research, theory modeling and numerical analysis.

The thermal crack problem has attracted a lot of attention in the experimental side. A. Yuse and M. Sano [2] firstly taken the experiment that heated a thin glass plate with a notch at its end and pulled in the cold bath (the similar experimental process model shows in Fig.1.0.1). The control parameters in this experiment are mainly the width of glass plate L, the different of temperature ΔT between the oven and cold bath and the pulling velocity v.

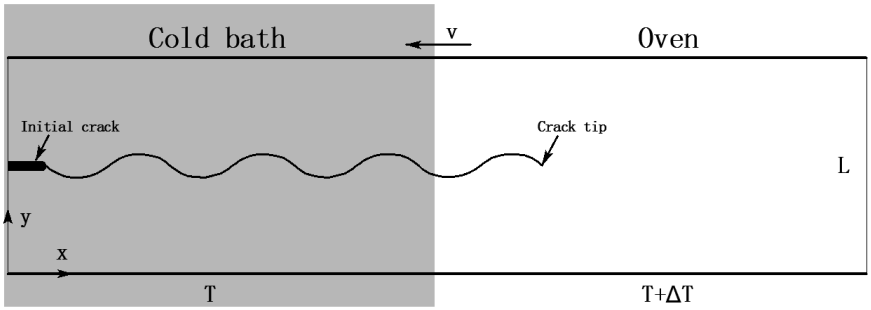

Figure 1.0.1: Experimental process model

The similar experiments were done by O. Ronsin and B. Perrin [9], Yang et al. [19] and Deegan et al [5]. The results show in Fig.1.0.2 that the crack does not propagate, the crack propagates

following a straight centered path and the crack propagates to oscillate with the different oscillating wavelength. Interestingly, these are very reproducible regimes, which makes the thermal crack an ideal model experiment as it allows to study the slow propagation of cracks under well controlled conditions.

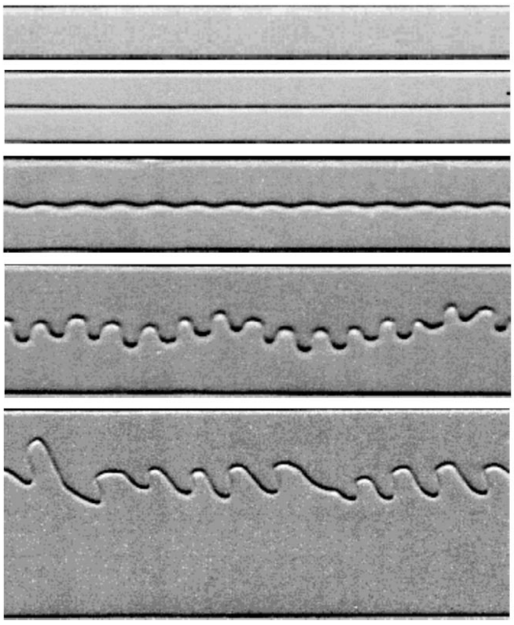

Figure 1.0.2: The various crack growth experiment [9]

Analytically and numerically the crack path prediction in the modeling system is an other important way to research this problem. However, this work is one of main challenges in the field of fracture mechanics, because a satisfactory equation of motion of a crack tip is associated with a fundamental understanding of material separation mechanisms that are showed by Freund [12] and Broberg [1]. There are some different crack propagation theories which have been done by scientists.

The general idea of crack propagation law is a pattern formation process induced by mechanical stresses. Within the framework of Linear Elastic Fracture Mechanics (LEFM), the propagation of a crack is mainly governed by the singular behavior of the stress field in the vicinity of its tip and this theories were done by Freund [12] and Leblond [17].

The Griffith energy criterion governs the evolution of the crack tip by the Griffith [15]. This law controls the states that the intensity of the loading necessary to induce propagation is given

by $G = \Gamma$, where G is the energy release rate and Γ is the fracture energy of material, that is the energy needed to create new free surfaces. The Irwin criterion [18] is a rewritten using the stress of Griffith criterion. This model is very useful in predicting crack initiation and it cannot predict the direction of the tip. The Principle of Local Symmetry (PLS) was first formulated by Barenblatt G. [13] and it states that the crack advances in much a way that in-plane shear stress vanishes in the vicinity of the crack tip. The PLS rule can achieve the shortage of the Griffith criterion. Recently there are many development laws of PLS to apply for the crack tip and prediction. And Katzav E. [7] used a pure LEFM approach combined with the Griffith criterion and the PLS to study roughening instabilities of crack.

In this work, we use the phase-field modeling and numerical analyze the crack propagation. The phase field model was firstly introduced by Caginalp G. and Fife P. [14]. F. Corson et al. [6] used the method to simulate the thermal crack problem Fig.1.0.1 and compared its results with those of a theoretical analysis.

The phase-field modeling is a based on the linearized elastodynamics [10] coupled the phase field modeling. Its detail is addressed in the next chapter. Here, I would like to address another important point that is wave propagation in the numerical crack propagation. The problem is that the velocity of each points of material is 0 at the beginning and the velocity is also very small in the quasistatic of crack propagation. However, the velocity is first derivative the displacement by the elastodynamics model. In other words, there are wave in crack propagation in numerical analysis. To reduce this effect, one way is to add the damping in the material when the crack is propagating, specially, the dynamics of quasistatic of crack propagation under the thermal loading.

This paper mainly includes the phase-field modeling of crack and numerical analysis in the chapter 2, the simple case of crack propagation under displacement loading in the chapter 3 and the dynamics of quasistatic of crack propagation in the chapter 4.

Chapter 2

The phase-field modeling of crack and numerical analysis

The phase field modeling is to introduce an additional field (the phase field) that describes the state of the system. The main advantage of this method is to get a clear shape of same phase value curve. In this work of fracture, the material is intact by $\phi = 1$ and crack by $\phi = 0$. The modeling is a linearized elastodynamics model coupling the phase theory in this work. It has the desired properties, couping between the phase field and elastic field, that no stresses are transmitted across a crack and on can associate a finite surface energy with the interface, so that the fracture energy is well-defined [6]. In this chapter, there are two parts that are evolution problems in elastic phase field modeling and numerical analysis of the evolution problem.

2.1 The phase field modeling

The phase field modeling is linearized elastodynamics [10] coupled the phase field. The displacement field is u_i. For small deformation in this problem, the strain ε_{ij} field is

$$\varepsilon_{ij} = \frac{1}{2}(\frac{\partial u_i}{\partial x_j} + \frac{\partial u_j}{\partial x_i}) \tag{2.1.1}$$

Considering an isotropic elastic material and the thermal loading, i.e. the constitutive law (the stress field σ_{ij}) is given by

$$\sigma_{ij} = \lambda tr\varepsilon_{kk}\mathbb{I}_{ij} + 2\mu\varepsilon_{ij} - K\alpha\Delta T\mathbb{I}_{ij} \tag{2.1.2}$$

where λ is the Lame Modulus, μ is the shear modulus, K is the bulk modulus in the two dimensional problem $K = \lambda + \mu$ [8], α is the thermal expansion coefficient and ΔT is the temperature change.

The acceleration, stress field σ_{ij} and phase field ϕ (it is a scalar) can be put in the linear momentum balance (balance equation), which reads

$$divg(\phi)\sigma_{ij} = \frac{d^2u_i}{dt^2} \tag{2.1.3}$$

$$g(\phi) = 4\phi^3 - 3\phi^4 \tag{2.1.4}$$

where u_i is displacement field, σ_{ij} is Cauchy stress field and ϕ ($0 \leqq \phi \leqq 1$) is phase field. The properties of function $g(\phi)$ are $g(0) = 0$, $g(1) = 1$ and $g^{'}(0) = g^{'}(1) = 0$. The function $g(\phi)$ couples in elastic energy by Adda-Bedia and Pomeau [3]. It means that, when the material is broken ($\phi = 0$), the elastic energy is 0 and, while the material is intact, it linearly contributes the elastic energy.

The free energy E_{el} of the body is a function of the strain tensor and the change the temperature of the body [16]. Since the free energy is a scalar, each term in the expansion of E_{el} must be a scalar also. The components of free energy are that $F_0(T)$ is a function of initial temperature T, $\frac{1}{2}\lambda(tr\varepsilon_{ij})^2$ is the squared sum of the diagonal strain tensor, $\mu tr\varepsilon_{ij}^2$ is the sum of diagonal the squares of strain and $-K\alpha\Delta T tr\varepsilon_{ij}$ is component of the temperature change. We therefore have as far as all terms:

$$E_{el} = F_0(T) - K\alpha\Delta T tr\varepsilon_{ij} + \frac{1}{2}\lambda(tr\varepsilon_{ij})^2 + \mu tr\varepsilon_{ij}^2 \tag{2.1.5}$$

The laws of thermodynamics are only directly applicable to systems in thermal equilibrium. In other words, the minimization of the free energy equals 0 that is thermal equilibrium systems. We change the form of the free energy to fit the minimization value 0. Here, an example of two dimensional problem (2D problem is following work) is showed by the allocation method.

Form of equation 2.1.5 is changed

$$E_{el} = F_0(T) - K\alpha\Delta T(\varepsilon_{xx} + \varepsilon_{yy}) + \frac{K}{2}(\varepsilon_{xx} + \varepsilon_{yy})^2 + \mu(2\varepsilon_{xy}^2 + \frac{1}{2}(\varepsilon_{xx} - \varepsilon_{yy})^2) \tag{2.1.6}$$

Eequation 2.1.6 is changed by the allocation method

$$E_{el} = F_0(T) + \frac{K}{2}((\varepsilon_{xx} + \varepsilon_{yy}) - \alpha\Delta T)^2 - \frac{K}{2}(\alpha\Delta T)^2 + \mu(2\varepsilon_{xy}^2 + \frac{1}{2}(\varepsilon_{xx} - \varepsilon_{yy})^2) \tag{2.1.7}$$

Let take the initial term $F_0(T) = \frac{K}{2}(\alpha\Delta T)^2$. The free energy E_{el} only has the squared terms which mean the minimization value always equals 0.

Finally, we obtain the free energy equation that is

$$E_{el} = \frac{K}{2}(\varepsilon_{xx} + \varepsilon_{yy} - \alpha\Delta T)^2 + \mu(2\varepsilon_{xy}^2 + \frac{1}{2}(\varepsilon_{xx} - \varepsilon_{yy})^2) \tag{2.1.8}$$

The phase field can be made to track the correct state if it obeys a standard two minimum Ginzburg-Landau equation with the relative energy of two wells dependent on $E_{el} - E_c$ [4]. Specifically, we choose

$$\frac{d\phi}{dt} = D_\phi \nabla^2 \phi - V_{DW}^{'}(\phi) - \frac{\mu}{2} g^{'}(\phi)(E_{el} - E_c) \tag{2.1.9}$$

where E_c is a constant value which represents the critical magnitude of the elastic energy. The basic idea involves representing the local state of the system, either intact with $E_{el} > E_c$ or broken with $E_{el} < E_c$. And where $V_{DW}(\phi) = \frac{1}{4}\phi^2(1-\phi)^2$, $V_{DW}^{'}(\phi) = \frac{1}{2}\phi - \frac{3}{2}\phi^2 + \phi^3$, $g^{'}(\phi) = 12\phi^2 - 12\phi^3$ and the constant D_ϕ is the diffuse coefficient.

2.2 Numerical analysis of the evolution problem

This problem is solved by numerical methods that are the Finite Differences Method for the space field and the Forward Euler Method for the time field. We get all initial fields and then we get the current all fields by those two methods. Specifically, we solve this problem by coding in the Fortran and plot the results by Matlab. Because the Fortran has good stability and fast and the Matlab has good the visibility.

2.2.1 Initial all fields

The numerical analysis is two dimensional (2D) problem. Given the initial finite element fields are the displacement field, phase field and temperature change field. For example, the numerical domain is $400 * 400$ grid points which mean $0 \leq x \leq n_x = 400$ and $0 \leq y \leq n_y = 400$ (x and y are integer). The part of grid points show in Fig.2.2.1. The displacement fields are u_x^n and u_y^n on the nodes $\bullet$ (marked nodes 1). For example, the displacement fields are

$$\begin{cases} u_x^n(x,y) = 0 \\ u_y^n(x,y) = (y - n_y/2 + 2.5)^2 \end{cases} \tag{2.2.1}$$

We mark each initial quantity is n and each current quantity $n+1$.

The phase field ϕ is on the nodes $\circ$ (marked nodes 2). For example, the phase field is

$$\phi^n(x,y) = 1 - (e^{-r^2/400}) * (1 + tanh((4n_x/8 - 5 - x)/5))/2 \tag{2.2.2}$$

where $r = (y - n_y/2 + 2.5)^2$.

And the temperature change field ΔT is on the nodes $\circ$ (marked nodes 2). For example, the temperature change field (also called tt) is

$$\begin{cases} \Delta T(x,y) = 0 & 0 \leq x < 200 \\ \Delta T(x,y) = -0.01 * tanh((200 - x)/12) + 0.01 & 200 \leq x \leq 400 \end{cases} \tag{2.2.3}$$

This field doesn't depend on y. In other words, the temperature field is constant value in the same y and it shows in the chapter 4.

We can see other nodes $\diamond$ (marked nodes 3) in the Fig.2.2.1. They help to solve some quantities which have relation between the two nodes 1 field and nodes 2 field. Therefore, we call the nodes 3 are caculated field.

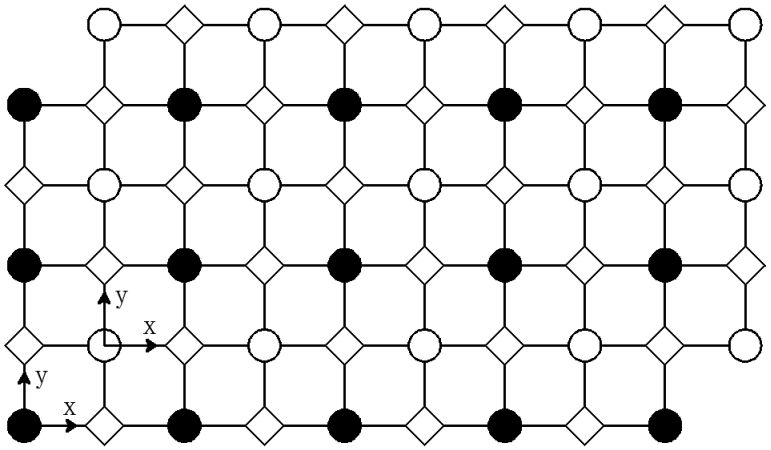

Figure 2.2.1: Grid points of different fields (• Nodes 1 - Displacement field; ◦ Nodes 2 - Phase field and temperature change field; ◇ Nodes 3 - Caculation field)

According to the phase field modeling, we can solve the initial strain fields. Firstly, the average values of initial displacement fields u_x^n on the nodes 3 are

$$\begin{cases} u_x^n(x,y)_{right} = 0.5 * (u_x^n(x+1,y) + u_x^n(x+1,y+1)) \\ u_x^n(x,y)_{left} = 0.5 * (u_x^n(x,y) + u_x^n(x,y+1)) \\ u_x^n(x,y)_{up} = 0.5 * (u_x^n(x,y+1) + u_x^n(x+1,y+1)) \\ u_x^n(x,y)_{down} = 0.5 * (u_x^n(x,y) + u_x^n(x+1,y)) \end{cases} \tag{2.2.4}$$

By the same way, we obtain the average values of initial displacement fields u_y^n on the nodes 3 that are

$$\begin{cases} u_y^n(x,y)_{right} = 0.5 * (u_y^n(x+1,y) + u_y^n(x+1,y+1)) \\ u_y^n(x,y)_{left} = 0.5 * (u_y^n(x,y) + u_y^n(x,y+1)) \\ u_y^n(x,y)_{up} = 0.5 * (u_y^n(x,y+1) + u_y^n(x+1,y+1)) \\ u_y^n(x,y)_{down} = 0.5 * (u_y^n(x,y) + u_y^n(x+1,y)) \end{cases} \tag{2.2.5}$$

Finite differences method (FDM) is numerical method for solving differential equation by approximating them with difference equations, in which finite differences approximate the derivatives. The derivation comes from Taylor's polynomial which is an approximation for the first

derivative of the function in this method [11]. FDM is thus discretization method and my project the initial fields are satisfied.

According to the strain equation 2.1.1, we can obtain the initial strain fields on the nodes 2 by the finite differences method that are

$$\begin{cases} \varepsilon_{xx}^n(x,y) = 0.5 * \frac{u_x^n(x,y)_{right} - u_x^n(x,y)_{left}}{dx} * 2 \\ \varepsilon_{xy}^n(x,y) = 0.5 * (\frac{u_x^n(x,y)_{up} - u_x^n(x,y)_{down}}{dy} + \frac{u_y^n(x,y)_{right} - u_y^n(x,y)_{left}}{dx}) \\ \varepsilon_{yy}^n(x,y) = 0.5 * \frac{u_y^n(x,y)_{up} - u_y^n(x,y)_{down}}{dy} * 2 \\ \varepsilon_{yx}^n(x,y) = 0.5 * (\frac{u_y^n(x,y)_{right} - u_y^n(x,y)_{left}}{dx} + \frac{u_x^n(x,y)_{up} - u_x^n(x,y)_{down}}{dy}) \end{cases} \tag{2.2.6}$$

According to the stress equation 2.1.2 and the initial strain fields, we obtain the initial stress fields on the nodes 2 are easily showed that are

$$\begin{cases} \sigma_{xx}^n(x,y) = \lambda(\varepsilon_{xx}^n(x,y) + \varepsilon_{yy}^n(x,y)) + 2\mu\varepsilon_{xx}^n(x,y) - K\alpha\Delta T(x,y) \\ \sigma_{xy}^n(x,y) = 2\mu\varepsilon_{xy}^n(x,y) \\ \sigma_{yy}^n(x,y) = \lambda(\varepsilon_{xx}^n(x,y) + \varepsilon_{yy}^n(x,y)) + 2\mu\varepsilon_{yy}^n(x,y) - K\alpha\Delta T(x,y) \\ \sigma_{yx}^n(x,y) = 2\mu\varepsilon_{yx}^n(x,y) \end{cases} \tag{2.2.7}$$

We can change the forms of two accelerations by the equation 2.1.3 that are

$$\begin{cases} \frac{d^2u_x^n(x,y)}{dt^2} = \partial_x(g(\phi^n(x,y))\sigma_{xx}^n(x,y)) + \partial_y(g(\phi^n(x,y))\sigma_{xy}^n(x,y)) \\ \frac{d^2u_y^n(x,y)}{dt^2} = \partial_y(g(\phi^n(x,y))\sigma_{yy}^n(x,y)) + \partial_x(g(\phi^n(x,y))\sigma_{yx}^n(x,y)) \end{cases} \tag{2.2.8}$$

Now we have equation 2.2.8 of stress fields and phase field on the nodes 2. However, we would like to get the results of acceleration on the nodes 1. Here, we can use the finite differences method again in the right sides to the two accelerations on the nodes 1.

Firstly, we need to get the average values of function $g(\phi)$ and the average value of stresses on the nodes 3 (Calculation field). To obtain the clear results, they are separately written that are

$$\begin{cases} g(\phi^n(x,y))_{right} = 0.5 * (g(\phi^n(x,y)) + g(\phi^n(x,y-1))) \\ g(\phi^n(x,y))_{left} = 0.5 * (g(\phi^n(x-1,y)) + g(\phi^n(x-1,y-1))) \end{cases} \tag{2.2.9}$$

and

$$\begin{cases} \sigma^n_{xx}(x,y)_{right} = 0.5 * (\sigma^n_{xx}(x,y) + \sigma^n_{xx}(x,y-1)) \\ \sigma^n_{xx}(x,y)_{left} = 0.5 * (\sigma^n_{xx}(x-1,y) + \sigma^n_{xx}(x-1,y-1)) \\ \sigma^n_{yx}(x,y)_{right} = 0.5 * (\sigma^n_{yx}(x,y) + \sigma^n_{yx}(x,y-1)) \\ \sigma^n_{yx}(x,y)_{left} = 0.5 * (\sigma^n_{yx}(x-1,y) + \sigma^n_{yx}(x-1,y-1)) \end{cases} \tag{2.2.10}$$

Then, we can obtain the values $\partial_x(g(\phi^n(x,y))\sigma^n_{xx}(x,y))$ and $\partial_x(g(\phi^n(x,y))\sigma^n_{yx}(x,y))$ on the nodes 1 by the finite differences method that are

$$\partial_x(g(\phi^n(x,y))\sigma^n_{xx}(x,y)) = \frac{g(\phi^n(x,y))_{right}\sigma^n_{xx}(x,y)_{right} - g(\phi^n(x,y))_{left}\sigma^n_{xx}(x,y)_{left}}{dx} \tag{2.2.11}$$

$$\partial_x(g(\phi^n(x,y))\sigma^n_{yx}(x,y)) = \frac{g(\phi^n(x,y))_{right}\sigma^n_{yx}(x,y)_{right} - g(\phi^n(x,y))_{left}\sigma^n_{yx}(x,y)_{left}}{dx} \tag{2.2.12}$$

By the same way, we have the average values of function $g(\phi)$ and the average value of stresses on the nodes 3 that are

$$\begin{cases} g(\phi^n(x,y))_{up} = 0.5 * (g(\phi^n(x,y)) + g(\phi^n(x-1,y))) \\ g(\phi^n(x,y))_{down} = 0.5 * (g(\phi^n(x,y-1)) + g(\phi^n(x-1,y-1))) \end{cases} \tag{2.2.13}$$

and

$$\begin{cases} \sigma^n_{yy}(x,y)_{up} = 0.5 * (\sigma^n_{yy}(x,y) + \sigma^n_{yy}(x-1,y)) \\ \sigma^n_{yy}(x,y)_{down} = 0.5 * (\sigma^n_{yy}(x,y-1) + \sigma^n_{yy}(x-1,y-1)) \\ \sigma^n_{xy}(x,y)_{up} = 0.5 * (\sigma^n_{xy}(x,y) + \sigma^n_{xy}(x-1,y)) \\ \sigma^n_{xy}(x,y)_{down} = 0.5 * (\sigma^n_{xy}(x,y-1) + \sigma^n_{xy}(x-1,y-1)) \end{cases} \tag{2.2.14}$$

We can obtain the values $\partial_y(g(\phi^n(x,y))\sigma^n_{yy}(x,y))$ and $\partial_y(g(\phi^n(x,y))\sigma^n_{xy}(x,y))$ on the nodes 1 by the FDM that are

$$\partial_y(g(\phi^n(x,y))\sigma^n_{yy}(x,y)) = \frac{g(\phi^n(x,y))_{up}\sigma^n_{yy}(x,y)_{up} - g(\phi^n(x,y))_{down}\sigma^n_{yy}(x,y)_{down}}{dy} \quad (2.2.15)$$

$$\partial_y(g(\phi^n(x,y))\sigma^n_{xy}(x,y)) = \frac{g(\phi^n(x,y))_{up}\sigma^n_{xy}(x,y)_{up} - g(\phi^n(x,y))_{down}\sigma^n_{xy}(x,y)_{down}}{dy} \quad (2.2.16)$$

According to equation 2.2.8, now we can get the two initial accelerations $\frac{d^2u^n_x(x,y)}{dt^2}$ and $\frac{d^2u^n_y(x,y)}{dt^2}$ on the nodes 1.

We can obtain the initial rate of phase $\frac{d\phi^n(x,y)}{dt}$ on the nodes 2 by the equation 2.1.9. There is a Laplace equation $\nabla^2\phi$ in the equation 2.1.9. And $dx = dy$ in this problem. To solve it, we use the skewed 9-point stencil (see Fig.).

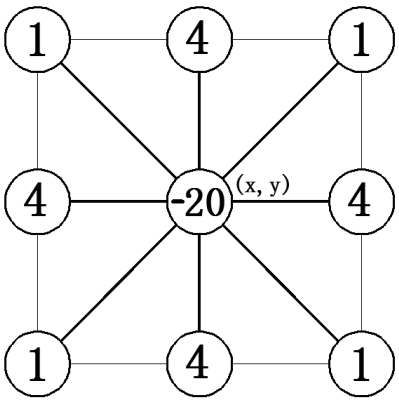

Figure 2.2.2: Skewed 9-point stencil

Therefore, the Laplace equation is

$$\begin{aligned}\nabla^2\phi^n(x,y) &= \frac{1}{6(dx)^2}(\phi^n(x-1,y-1)+4\phi^n(x-1,y)+4\phi^n(x+1,y)\\ &\quad +\phi^n(x+1,y+1)-20\phi^n(x,y)+\phi^n(x+1,y-1)\\ &\quad +4\phi^n(x,y-1)+4\phi^n(x,y+1)+\phi^n(x-1,y+1)) \quad (2.2.17)\end{aligned}$$

We have the initial strain fields and phase field on the nodes 2 and we can easily get the E_{el} and $V'_{Dw}(\phi)$. Then, according to the equation 2.1.9, we obtain the initial rate of phase $\frac{d\phi^n(x,y)}{dt}$ on the nodes 2.

2.2.2 Current all fields

We obtain the two initial accelerations $\frac{d^2u_x^n(x,y)}{dt^2}$ and $\frac{d^2u_y^n(x,y)}{dt^2}$ on the nodes 1 and the initial rate of phase $\frac{d\phi^n(x,y)}{dt}$ on the nodes 2 in before subsection. The current displacement fields $u_x^{n+1}(x,y)$, $u_y^{n+1}(x,y)$ and the current phase field $\phi^{n+1}(x,y)$ is solved by the Forward Euler Method.

This method is a numerical procedure for solving ordinary differential equations with a given initial value. It is the most basic explicit method for numerical integration of ordinary differential equations and is the simplest Runge–Kutta method [11].

The initial velocities are $\frac{du_x^n(x,y)}{dt} = 0$ and $\frac{du_y^n(x,y)}{dt} = 0$. We obtain the current velocities on the nodes 1 by the Forward Euler Method that are

$$\frac{du_x^{n+1}(x,y)}{dt} = \frac{du_x^n(x,y)}{dt} + \frac{d^2u_x^n(x,y)}{dt^2}dt \tag{2.2.18}$$

$$\frac{du_y^{n+1}(x,y)}{dt} = \frac{du_y^n(x,y)}{dt} + \frac{d^2u_y^n(x,y)}{dt^2}dt \tag{2.2.19}$$

Because the initial velocities are 0, we use the current velocities to replace the initial velocities to solve the current displacement fields $u_x^{n+1}(x,y)$ and $u_y^{n+1}(x,y)$ on the nodes 1 by the Forward Euler Method again that are

$$u_x^{n+1}(x,y) = u_x^n(x,y) + \frac{du_x^{n+1}(x,y)}{dt}dt \tag{2.2.20}$$

$$u_y^{n+1}(x,y) = u_y^n(x,y) + \frac{du_y^{n+1}(x,y)}{dt}dt \tag{2.2.21}$$

The current phase field $\phi^{n+1}(x,y)$ is easily got by the Forward Euler Method that is

$$\phi^{n+1}(x,y) = \phi^n(x,y) + \frac{d\phi^n(x,y)}{dt}dt \tag{2.2.22}$$

Now we have the current displacement fields $u_x^{n+1}(x,y)$ and $u_y^{n+1}(x,y)$, the current phase field $\phi^{n+1}(x,y)$ and the constant temperature change field $\Delta T(x,y)$. We also get current all fields same as the initial all fields. By the same way, we can obtain all fields in the next step. Therefore, this problem is solved by code and we code by Fortran in this project.

Chapter 3

The simple case of crack propagation under displacement loading

Firstly, we simulate a simple case of crack propagation under only displacement loading in this chapter. It looks like a tensile stress normal to the plane of the crack (by the Mode I fracture) to see the crack propagation. It would help to understand the phase modeling which shows in the chapter 2 and to check the code whether work.

3.1 Introduction of simulation

The grid points of domain (See Fig.3.1.1) are $800 * 400$ (It means $n_x = 800$ and $n_y = 400$).

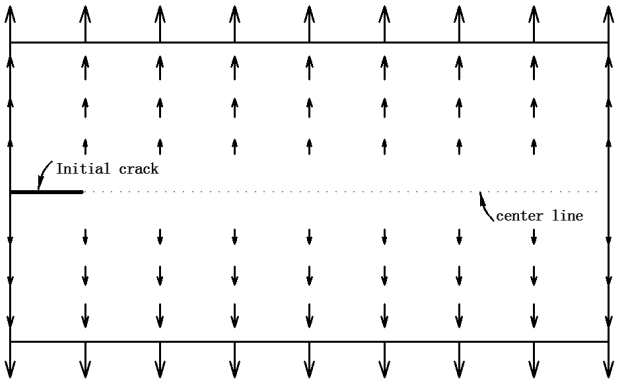

Figure 3.1.1: Initial crack and displacement field

The initial crack is in left and center of the domain and its size is $100 * 8$ grid points (Equation 3.1.1). Each grid size is $dx = dy = 0.2$.

$$\phi^n(x,y) = 1 - (e^{-r^2/400}) * (1 + tanh((n_x/8 - 5 - x)/5))/2 \tag{3.1.1}$$

where $r = (y - n_y/2 + 2.5)^2$.

The loading is displacement loading in the displacement field (See the equation 3.1.2). The loading is only apply in the y direction and the field also shows in Fig.3.1.1.

$$\begin{cases} u_x = 0 \\ u_y = (y - 200)/400 * \eta \end{cases} \tag{3.1.2}$$

Where η is the amplitude of displacement.

The left side is the mirror boundary for the displacements that mean $u_x(0,:) = -u_x(1,:)$ and $u_y(0,:) = u_y(1,:)$.

In this simulation, there is no temperature loading $\Delta T = 0$. Other parameters are that the time step $dt = 0.002$, the diffusion coefficient $D_\phi = 1$, Lame Modulus $\lambda = 1$, Shear modulus $\mu = 1$, thermal coefficient $\alpha = 1$ and constant $E_c = 1$.

3.2 The results of simulation

Firstly, the results are the straight crack propagation, when the amplitude of displacement $\eta = 20$. The crack shapes in the different time show in the Fig.3.2.1. The initial crack is not exactly in the center (about $y = 198$), while time $t = 1$. The width of crack decreases a little bit and increases to the initial width showed in $t = 100$. Then, the crack keeps a same width to propagate and the center increases a little bit (about $y = 198.3$) in $t = 200$. When $t = 300$, the crack reaches the right side.

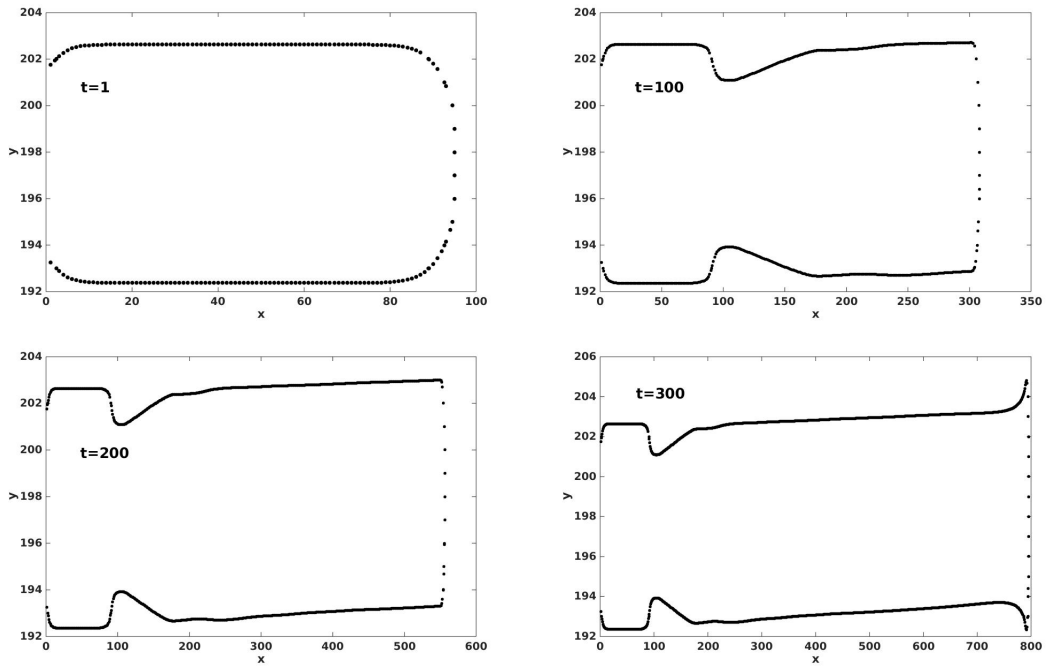

Figure 3.2.1: Crack propagation in different time

The x position of crack tip with time t shows in Fig.3.2.2. The crack is no propagation at beginning $t \leq 10$, and it reaches $x = 800$ about $t = 300$. Now, we give a definition of velocity of crack propagation that is the slope of curve (in Fig.3.2.2) timed $dx = 0.2$. We get the velocity of crack propagation is 0.495.

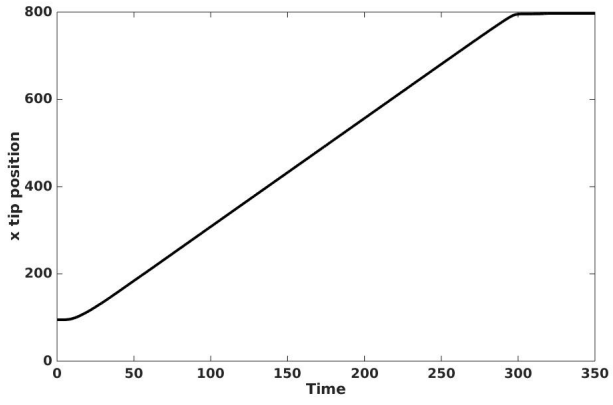

Figure 3.2.2: x tip position with time

Another simulation is branched crack propagation in Fig.3.2.3, while the $\eta = 30$. The in initial crack is same as the $\eta = 20$ in time $t = 1$. The width of crack increases from about 5 grid points to 30 grid points (as a torn shape) in $t = 50$. Then, the crack changes to two symmetrical branches and propagates in $t = 100$, $t = 150$ and $t = 200$.

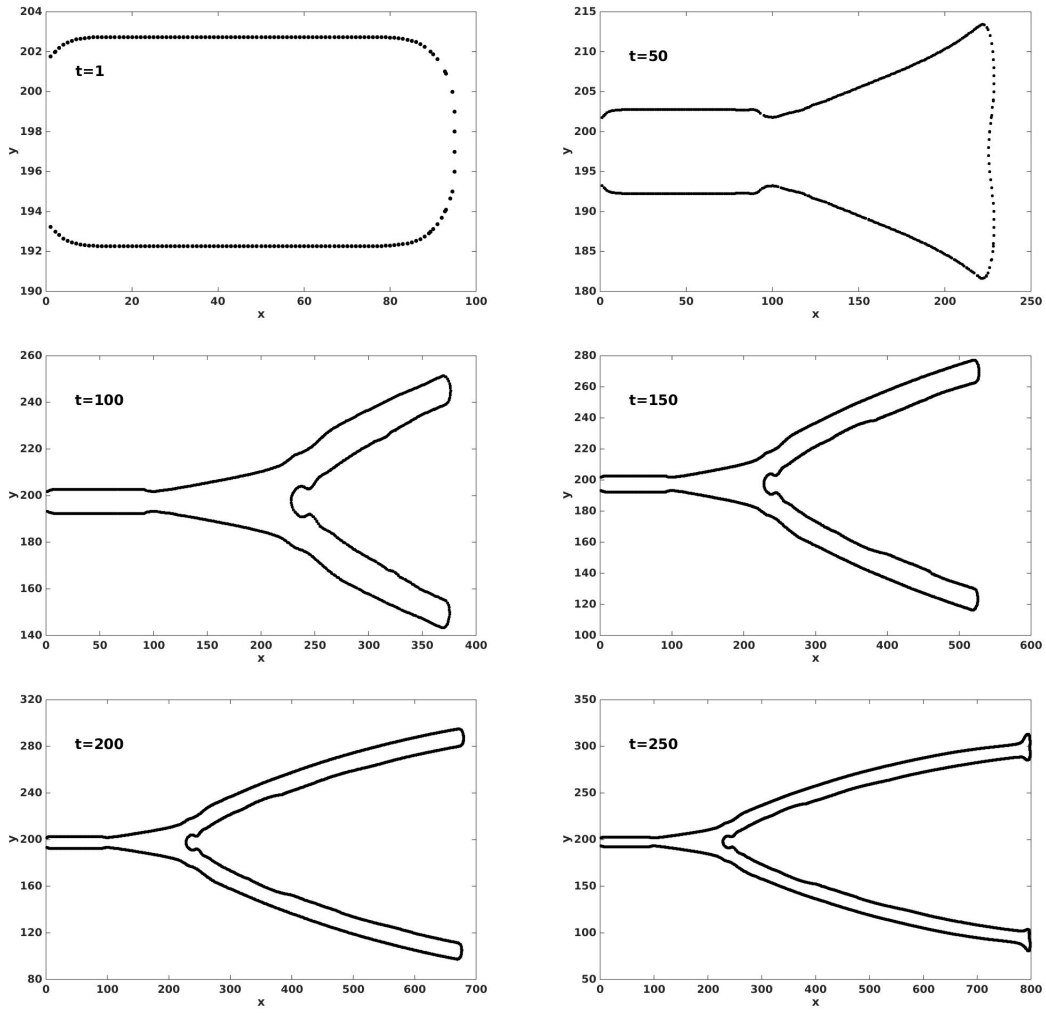

Figure 3.2.3: Crack propagation in different time

The x tip position with time shows in Fig.3.2.4. The crack starts to propagate at $t = 5$ and it reaches the right side at $t = 240$. The velocity of crack propagation keeps a constant value that is 0.599.

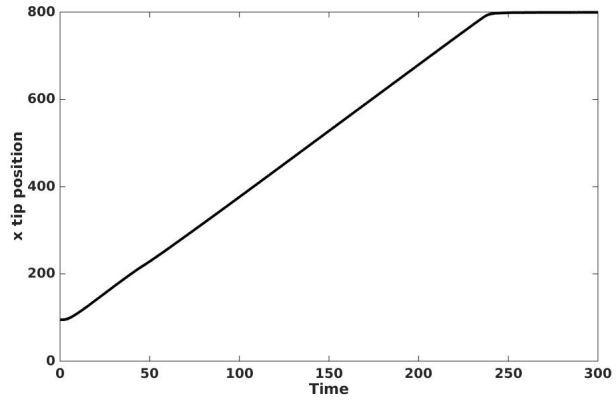

Figure 3.2.4: x tip position with time

Finally, we get the velocity of crack propagation in different amplitude of displacement η shown in Fig.3.2.5. The velocity is increasing with the amplitude increasing and this curve is closely linear relation. When the amplitude of the displacement is 16, the velocity is 0.374. The velocity is 0.626, while the amplitude is 32.5.

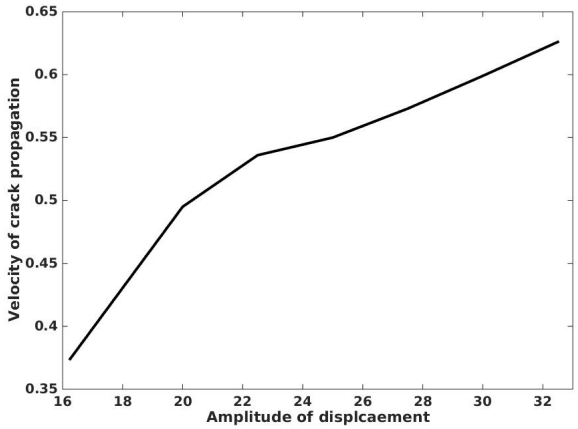

Figure 3.2.5: Velocity of crack with the amplitude of displacement

In this chapter, we get that the crack is straight crack propagation in the smaller displacement loading and the branched crack propagation in the higher displacement loading. And the velocity of crack propagation is increasing with the amplitude increasing. The phase field modeling and the code is working for the crack propagation.

Chapter 4

The dynamics of quasistatic of crack propagation

According to O. Ronsin and B. Perrn's experimental [9], the main two types of dynamics of quasistatic directional crack growth in brittle material are straight propagation and oscillating propagation. In this chapter, we simulated the two types of crack propagating under thermal loading. This work basics on before work which I have.

4.1 Introduction of simulation

This this chapter, the simulation domain is infinite length x and y=200 grid points of width. However, we only numerically simulate the finite domain that the grid points are $400 * 200$ each time step. To simulate the infinite length sample, the way is to move all domain right to left one grid each 2000 time steps (The time step is $dt = 0.002$). It looks like to pull a infinite length sample to left. The size of each grid is $dx = dy = 0.2$. We mark the initial crack left side $x = 0$ any time.

The initial crack (See Fig.4.1.1) equation is

$$\phi^n(x,y) = 1 - (e^{-r^2/200}) * (1 + tanh((n_x/1.29 - 5 - x)/5))/2 \tag{4.1.1}$$

where $r = (y - n_y * 0.524 + 2.5)^2$.

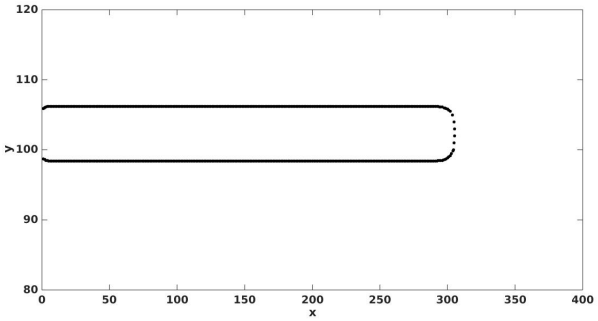

Figure 4.1.1: Initial crack

The thermal loading equation is

$$\begin{cases} \Delta T(x,y) = 0 & 0 \leq x < 200 \\ \Delta T(x,y) = -0.01 * tanh((200-x)/12) + 0.01 & 200 \leq x \leq 400 \end{cases} \tag{4.1.2}$$

This is a basic temperature shape in Fig.4.1.2. We need to time a amplitude γ in the simulation. This temperature is to simulate the problem Fig.1.0.1 that is hated the thin glass plate and pulled in cold bath.

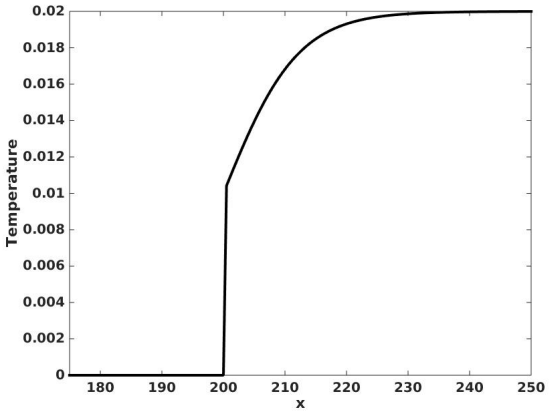

Figure 4.1.2: Basic temperature shape

There are free boundary conditions for the three sides. It means that, when $x = 1$ in the left

side, the $\sigma_{xx} = \sigma_{xy} = \sigma_{yx} = 0$ and

$$\begin{cases} \varepsilon_{yy} = \frac{u_y(0,y+1) - u_y(0,y)}{dy} \\ \varepsilon_{xx} = (K\alpha \triangle T - \lambda \varepsilon_{yy})/(2\mu + \lambda) \\ \sigma_{yy} = 2\mu(\varepsilon_{yy} - \varepsilon_{xx}) \end{cases} \tag{4.1.3}$$

By the same way, we have the free boundary conditions for up and down and down ($y = 0$ and $y = n_y$) that $\sigma_{xx} = 2\mu(\varepsilon_{xx} - \varepsilon_{yy})$. For each 2000 time steps, we simulate the pulled case of infinite sample that is

$$\begin{cases} u_x(x,y) = u_x(x+1,y) \\ u_y(x,y) = u_y(x+1,y) \\ \phi(x,y) = \phi(x+1,y) \end{cases} \tag{4.1.4}$$

As we mentioned in the introduction of wave propagation, we add the damping in each time step to reduce the velocity $\frac{du}{dt}$ equations 2.2.18 and 2.2.19 that

$$\frac{du_x^{n+1}(x,y)}{dt} = \frac{du_x^n(x,y)}{dt} + \frac{d^2u_x^n(x,y)}{dt^2}dt - f\frac{du_x^n(x,y)}{dt}dt - 0.2(1-\phi^n(x,y))\frac{du_x^n(x,y)}{dt}dt \tag{4.1.5}$$

$$\frac{du_y^{n+1}(x,y)}{dt} = \frac{du_y^n(x,y)}{dt} + \frac{d^2u_y^n(x,y)}{dt^2}dt - f\frac{du_y^n(x,y)}{dt}dt - 0.2(1-\phi^n(x,y))\frac{du_y^n(x,y)}{dt}dt \tag{4.1.6}$$

where f is a function and it depends on the position that means , when the position is far from crack center, there are more damping value.

Other parameters are that the time step $dt = 0.002$, the diffusion coefficient $D_\phi = 1$, Lame Modulus $\lambda = 1$, Shear modulus $\mu = 1$, thermal coefficient $\alpha = 1$ and constant $E_c = 1$.

4.2 Straight crack propagation

The amplitude of temperature is $\gamma = 350$, the crack propagation is straight crack (See Fig.4.2.1). The crack tip of y is between 100.81 to 100.86 and this tip is max elastic energy position.

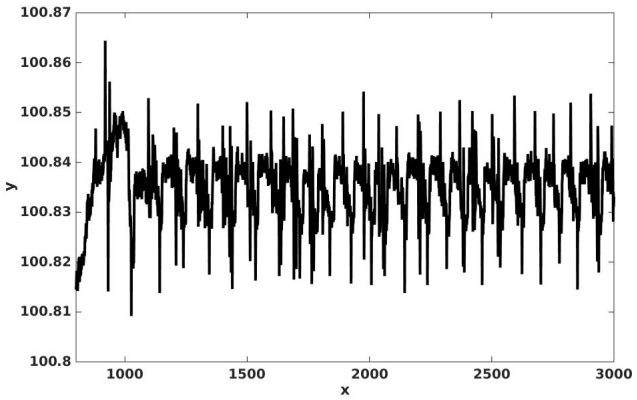

Figure 4.2.1: Crack tip position

The crack propagation in different time figures show in Fig. 4.2.2. At time t=4, the crack does not propagate and it about starts on t=125. The width of crack decreases from 8 to 7 (see t=1000). Then the crack keeps perfect line propagation and the shape doesn't change (See t=5000 and t=10000).

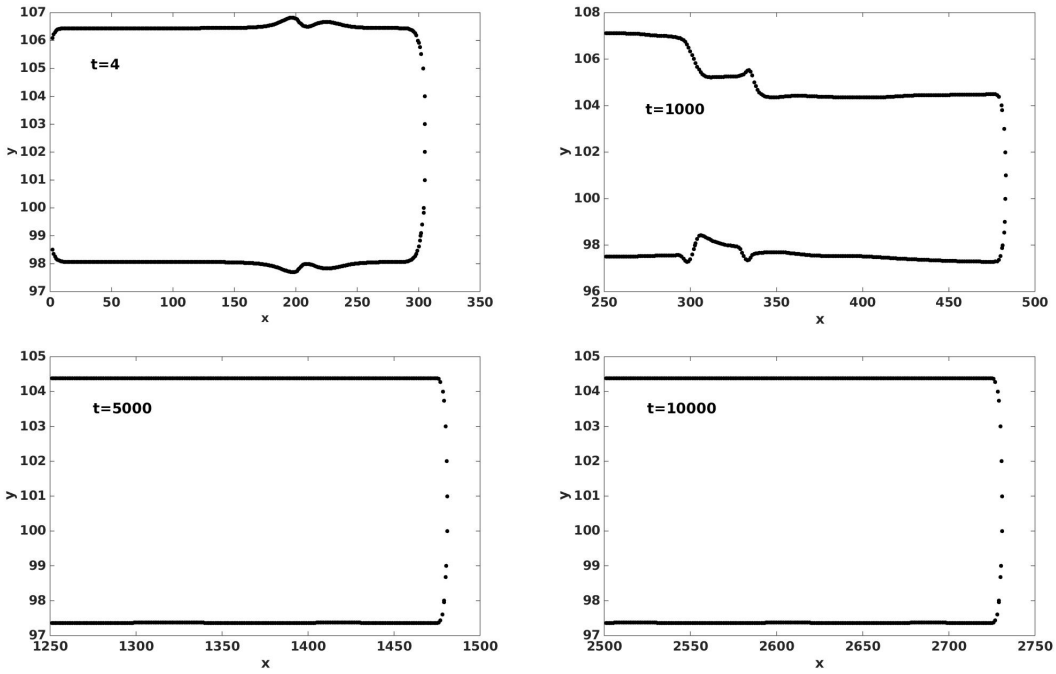

Figure 4.2.2: Crack propagation in different time

4.3 Oscillating crack propagation

The max amplitude of temperature is $\gamma = 500$ and the amplitude starts 400 linearly increased to 500 with the time step at the beginning time $t \leq 2000$. The crack propagation is oscillating propagation (max elastic energy position) Fig.4.3.1. The oscillation amplitude is increased with increasing the amplitude of temperature at beginning. The oscillation amplitude is closely a constant value about 15 after the time 2000 (it means the max temperature amplitude is constant value 500) at the crack position x about at 900.

The figure 4.3.1 show the crack is different architect's scale of the coordinates. An other words, the x coordinate is about 100 times of y coordinate. It is better to see the detail of shape of crack in the same scale of coordinates. We choose the two parts 1 and 2 in Fig.4.3.1 which represent the two different shape in Fig.4.3.1.

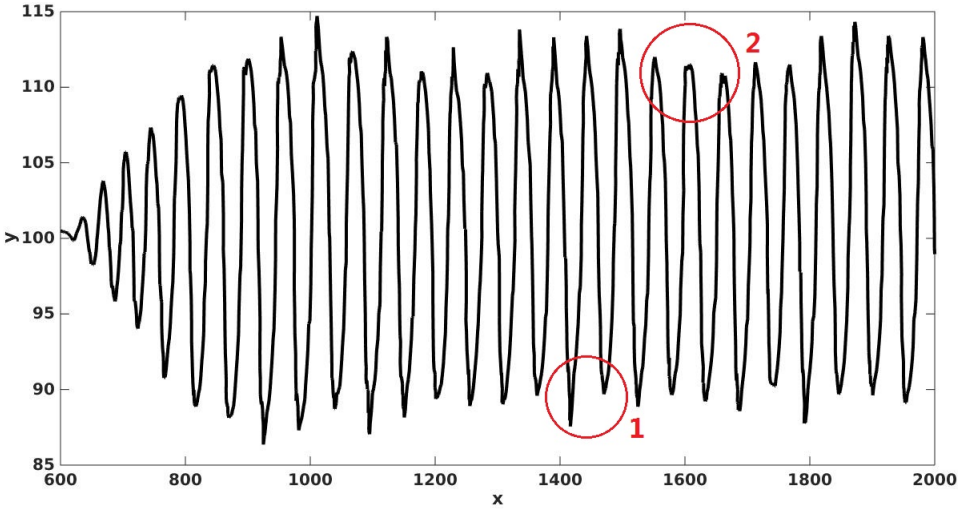

Figure 4.3.1: Crack tip position

The detail of parts 1 and 2 shown in Fig.4.3.2. This results of crack shape are similar with experimental and numerical results [9][6]. The oscillating wavelength is about 60 and the amplitude of oscillating is about 25 (between 85 to 115). The details of domain 1 and 2 are similar shape.

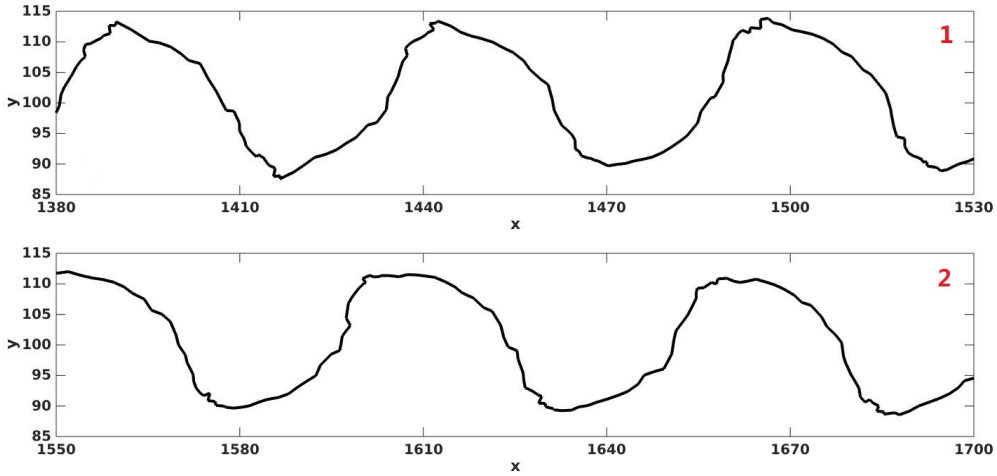

Figure 4.3.2: Parts of crack with the same architect's scale coordinates

The real phase crack shape shows in Fig.4.3.3 in different time. At the beginning, the crack is straight propagation until the tip position is about the 620 (time is t=1280) (See the Fig.4.3.1). And the temperature amplitude is about $\gamma = 464$. Then the crack is oscillating and the amplitude of oscillating is increasing until the time t=2000 (x position x=800) temperature amplitude 500 (See the time t=2000, t=2500 and t=3000 in Fig.4.3.3).

From the Fig. 4.3.1, we found the amplitude of oscillating is also a litter increasing to t=2200 (x position x=850) and the amplitude of the oscillation doesn't change too much (y position is about 88 to112) which show in time t=5000 and t=10000 in Fig.4.3.3. If we see those phase crack in in same architect's scale of the coordinates, the amplitude of oscillating is similar and it is prefect oscillating in Fig.4.2.2.

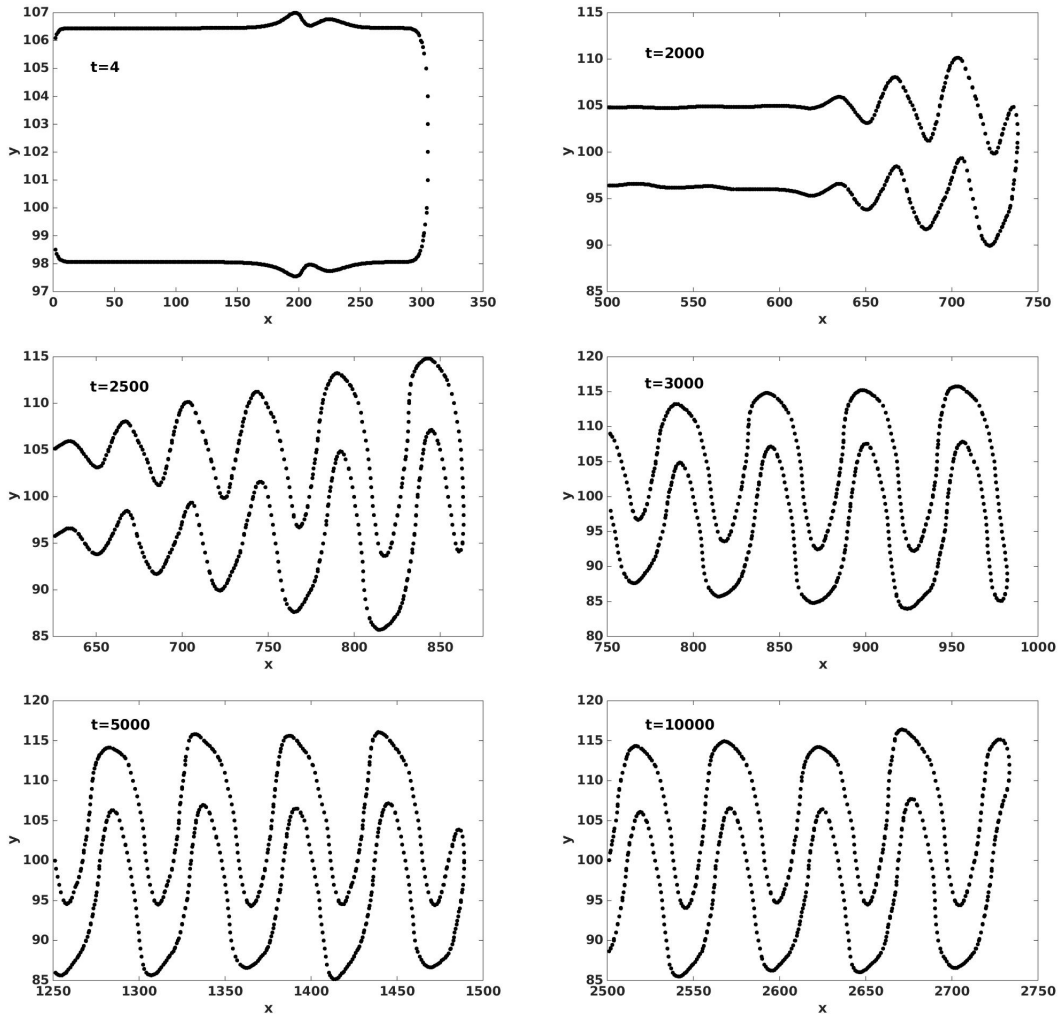

Figure 4.3.3: Crack propagation in different time

When the amplitude of temperature is $\gamma = 545$, the oscillating crack oscillating propagation little change (See Fig.4.3.4). The oscillating starts at about $x = 900$ and the amplitude of oscillating is increasing. Then it keeps a same value. However, the crack propagation little back and tip turns to one side. Then the crack back to center and going on the oscillating at about $x = 1200$.

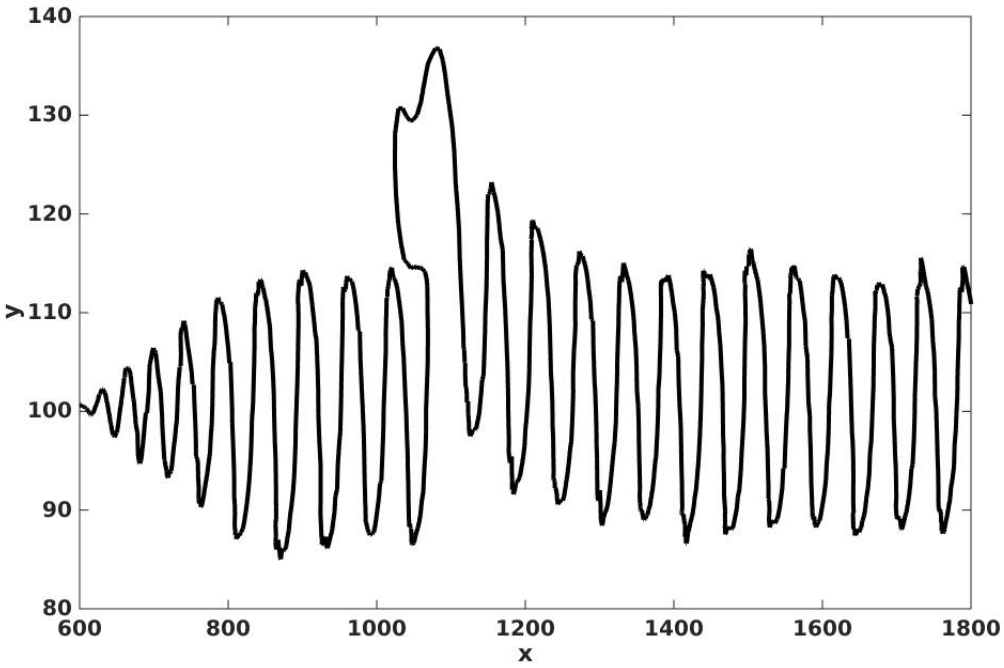

Figure 4.3.4: Crack tip position

The detail of different crack propagation shows in Fig.4.3.5 and it is max elastic energy position (it is part of crack in Fig.4.3.4). Now the crack is same architect's scale coordinates and we can find the detail of crack shape. The crack turn back about at $x = 1070$. The crack tip goes to left at $x = 1025$ and then it backs to right. When the tip $x = 1400$ (See Fig.4.3.4), the crack backs the normal oscillating.

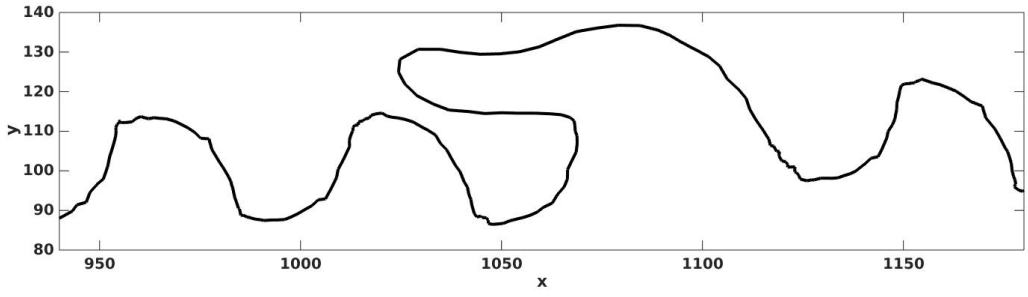

Figure 4.3.5: Part of crack with the same architect's scale coordinates

The phase crack in different time shows in Fig.4.3.6. When $t = 3352$, the crack starts to back

left. The strang propagation is fast and it reaches the before back is only time 20 See $t = 3372$. Then it spends time to propagate $t = 3460$ to one side and to right. Finally, we find the crack back to normal propagation (when the tip after 1200).

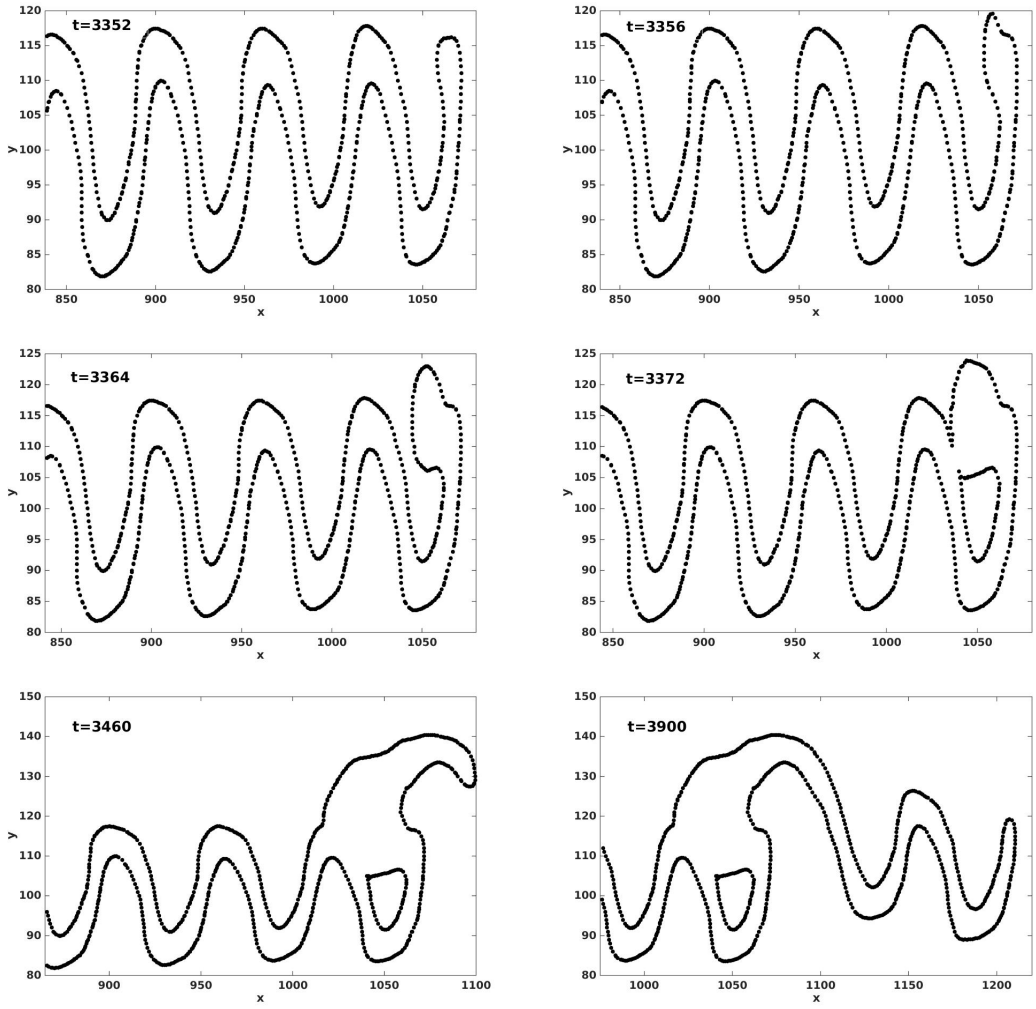

Figure 4.3.6: Crack propagation in different time

However, the phase crack propagate to back and it confuses with the previous crack $t = 3372$ and $t = 3460$ in Fig.4.3.6. To solve this problem, we need to get the result that has longer wavelength of oscillating.

Chapter 5
Conclusions

This work starts the phase field modeling that is intact $0.5 \leq \phi \leq 1$ and crack by $0 \leq \phi \leq 0.5$. This problem is solved by the numerical methods which mainly are Finite Differences Method for the space field and the Forward Euler Method for the time field. Then, we code this problem by Fortran program. The first results are straight crack and symmetric branched crack by a simple case under the displacement loading.

The main results are straight propagation and oscillating propagation under the thermal loading. We get all those two results in different amplitude of temperature that are $\gamma = 350$ and $\gamma = 500$ which fit other experimental and numerical research. The wavelength of oscillating is about 60 and amplitude of oscillating is 25. When the $\gamma = 545$, the oscillating crack would propagate a little back and it is going on oscillating propagation.

The future work is simulation of crack back case with the longer wavelength of oscillating and those results are compared with results from another approach, such as X-FEM.

Bibliography

[1] K.B. Broberg. *Cracks and Fracture*. Academic Press, London, 1999.

[2] A. Yuse el al. Transition between crack patterns in quenched glass plates. *Nature*, 362:329–331, 1993.

[3] Adda-Bedia M. el al. Crack instabilties of a heated glass strip. *Physical Review E*, 52(4):4105–4113, 1995.

[4] Alain Karma el al. Phase-field model of mode iii dynamic fracture. *Physical Review Letters*, 87(4):1–4, 2001.

[5] Deegan R. D. el al. Wavy and rough cracks in silicon. *Physical Review E*, 67:066209, 2003.

[6] F. Corson el al. Thermal fracture as a framework for quasi-static crack. *International Journal of Fracture*, 158:1–14, 2009.

[7] Katzav E. el al. Fracture surfaces of heterogeneous materials: a 2d solvable model. *Europhys. Lett.*, 78:46006, 2007.

[8] L. Monette el al. Elastic and fracture properties of the two-dimensional triangular and square lattices. *Modelling and Simulation in Materials Science and Engineering*, 2(1):53–66, 1994.

[9] O. Ronsin el al. Dynamics of quasistatic directional crack growth. *Physical Review E*, 58(6):7878–7886, 1998.

[10] Reza Abedi el al. *IUTAM Symposium on Discretization Methods for Evolving Discontinuities*, volume 5. Springer, The Netherlands, 2007.

[11] William el al. *Numerical recipes*. Cambridge University Press, England, 1986.

[12] L.B. Freund. *Dynamic Fracture Mechanics*. Cambridge University Press, England, 1990.

[13] Barenblatt G. On brittle cracks under longitudinal shear. *International Journal of Fracture*, 25(6):1110–1119, 1961.

[14] Caginalp G. and Fife P. Phase field methods for interfacial boundaries. *Physical Review B*, 33(11):7792–7794, 1986.

[15] A. A. Griffith. The phenomenon of rupture and flow in solid. *Philosophical Transactions of the Royal Society of London. Series A*, 221:163–198, 1920.

[16] L.D. Landau. *Theory of Elasticity*. Institute of Physical Problems, USSR Academy of Sciences, Moscow USSR, 1986.

[17] J.B. Leblond. *Mecanique de la rupture fragile et ductile*. Hermes Science Publications, Paris, 2003.

[18] Irwin G. R. Analysis of stresses and strains near the end of a crack traversing a plate. *Journal of Applied Mechanics*, 24:361–364, 1957.

[19] Ravi Chandar K. Yang B. Crack path instabilities in a quenched glass plate. *Journal of the Mechanics and Physics of Solids*, 49:91–130, 2001.